Journal of Solid State Chemistry 182 (2009) 1229–1234

Contents lists available at ScienceDirect

Journal of Solid State Chemistry

journal homepage: www.elsevier.com/locate/jssc

Sol–gel synthesis of nanocomposite materials based on lithium niobate nanocrystals dispersed in a silica glass matrix

Elisa Marenna [a], Carmela Aruta [b], Esther Fanelli [a], Mario Barra [b], Pasquale Pernice [a], Antonio Aronne [a,*]

[a] Dipartimento di Ingegneria dei Materiali e della Produzione, Università di Napoli Federico II, Piazzale V. Tecchio, 80125 Napoli, Italy
[b] CNR-INFM Coherentia e Dipartimento di Fisica, Università di Napoli Federico II, Complesso Universitario Monte S. Angelo, Via Cintia, 80126 Napoli, Italy

ARTICLE INFO

Article history:
Received 5 November 2008
Received in revised form
5 February 2009
Accepted 16 February 2009
Available online 26 February 2009

Keywords:
Sol–gel
Nanocomposites
$LiNbO_3$

ABSTRACT

With the final goal to obtain thin films containing stoichiometric lithium niobate nanocrystals embedded in an amorphous silica matrix, the synthesis strategy used to set a new inexpensive sol–gel route to prepare nanocomposite materials in the Li_2O–Nb_2O_5–SiO_2 system is reported. In this route, $LiNO_3$, $NbCl_5$ and $Si(OC_2H_5)_4$ were used as starting materials. The gels were annealed at different temperatures and nanocrystals of several phases were formed. Futhermore, by controlling the gel compositions and the synthesis parameters, it was possible to obtain $LiNbO_3$ as only crystallizing phase. $LiNbO_3$–SiO_2 nanocomposite thin films on Si–SiO_2 and Al_2O_3 substrates were grown. The $LiNbO_3$ average size, increasing with the annealing temperature, was 27 nm for a film of composition $10Li_2O$–$10Nb_2O_5$–$80SiO_2$ heated 2 h at 800 °C. Electrical investigation revealed that the nanocrystals size strongly affects the film conductivity and the occurrence of hysteretic current–voltage curves.

1. Introduction

Lithium niobate ($LiNbO_3$, LN) is a ferroelectric and non-linear optical material widely used in integrated and waveguides optics as well as in piezoelectric applications. According to the Li_2O–Nb_2O_5 phase diagram [1], LN has a wide solid solution region extending from the Nb-rich side (Li/[Nb+Li] about 0.47) to the stoichiometric point (Li/[Nb+Li] = 0.50). The congruent composition of LN exists between 48.35 and 48.65 mol% Li_2O. Therefore, when this material is obtained from high temperature processes, such as single-crystal Czochralski growth, non-stoichiometric crystals with Li_2O deficiency are generally obtained [2,3]. Stoichiometric LN (SLN), mainly in film shape, are more easily obtained by low temperature wet chemical techniques, among them the sol–gel [4–11]. The stabilization of Nb^{5+} ion in an aqueous environment is the key-step of any sol–gel route involving niobium. Hirano and co-workers [4,5] starting from an alcoholic solution of lithium–niobium ethoxide, $LiNb(OC_2H_5)_6$, have utilized the high reactivity of Nb^{5+} ion in an aqueous environment to obtain a solution of mixed lithium–niobium hydroxide, $LiNb(OH)_6$, from which thin crystalline films of SLN are obtained by dip-coating. The need of handling the precursors under a dry inert atmosphere and the precise control of the hydrolysis step are the main disadvantages of this procedure (that is called "double alkoxide"). An innovation in this sol–gel route, the addition of hydrogen peroxide solution to the alcoholic solution of lithium–niobium ethoxide, has been introduced by Cheng et al. [6] obtaining a slight improvement of the precursors handling and a lower temperature processing as well. Alternatively, the Nb^{5+} ion can be stabilized in aqueous solution by means of chelating and/or complexing agents, such as acetylacetone [7], malic acid [8], and citric acid [9].

The easy achievement of nanocrystalline LN is another advantage of the wet chemical techniques [9–11]. Nanocrystalline LN particles of about 20 nm dispersed in a silica matrix (20% by weight), with a grains structure very similar to that of the bulk material but with enhanced transport properties, have been obtained by the "double alkoxide" route [10]. It was shown that SiO_2 plays a key role to prevent the growth of nanocrystals by hindering their coarsening also at high temperature [11]. By the same route LN–SiO_2 sol–gel films, with LN/SiO_2 molar ratio equal to 1, have been synthesized by Bescher et al. [12]. Films annealed 2 h at 200 °C appeared transparent and exhibited a ferroelectric-like behavior even if they were amorphous to XRD. This behavior was related to the presence in the silica matrix of nanoclusters with size of 3–5 nm (named "ferrons") as revealed by HRTEM pictures, that the authors considered nanocrystallites-like [12]. Recently, LN–SiO_2 glass–ceramics with a LN content changing from 4 to 6 mol% have been synthesized by Graça et al. [13–15] in flakes shape using a sol–gel route that can be considered a slight modification of that proposed in Ref. [6]. It was found that in the samples subjected to electric gradient of 1000 kV m^{-1} the crystallization of LN started to occur at 650 °C while in absence of electrical field it occurred at 700 °C [13]. Moreover, in the

* Corresponding author. Fax: +39 081 76 82595.
E-mail address: anaronne@unina.it (A. Aronne).

0022-4596/$ - see front matter © 2009 Elsevier Inc. All rights reserved.
doi:10.1016/j.jssc.2009.02.022

600–800 °C range besides $LiNbO_3$ also cristobalite, $Li_2Si_2O_5$ and Li_3NbO_4 were found to crystallize [15].

The main aim of this work is to tune a new sol–gel route to synthesize nanocomposite materials in the Li_2O–Nb_2O_5–SiO_2 system. In the proposed method only silicon is introduced as alkoxide. The final goal has been the synthesis of transparent thin film containing lithium niobate nanocrystals embedded in a silica matrix.

2. Experimental

Lithium–niobium–silicon mixed-oxides were obtained by a suitable modification of the sol–gel route proposed in a recent paper [16] to synthesize mixed-oxides in the binary system Nb_2O_5–SiO_2. In this synthesis the hydrochloric acid plays the double role of catalyst and of complexing agent of Nb^{5+} ion allowing to achieve easily a stable and homogeneous solution.

Table 1
Gels composition (mol%) and crystallizing phases.

Sample	Li_2O	Nb_2O_5	SiO_2	Crystallizing phases
Bulk *B*-LN5	5	5	90	Cristobalite, $LiNbO_3$, T-Nb_2O_5, $LiNb_3O_8$
Bulk *B*-LN10	10	10	80	$LiNbO_3$, T-Nb_2O_5, $LiNb_3O_8$
Flakes *F*-LN10	10	10	80	$LiNbO_3$
Flakes *F*-LN15	15	15	70	$LiNbO_3$, $LiNb_3O_8$
Thin film *TF*-LN10	10	10	80	$LiNbO_3$

Lithium nitrate, $LiNO_3$ (99%, Gelest), niobium chloride, $NbCl_5$ (99%, Gelest) and tetraethoxysilane, $Si(OC_2H_5)_4$ (99%, Gelest), were used as starting materials in the sol–gel synthesis. Since the ultimate aim was the production of $LiNbO_3$ nanocrystals, in all the synthesis the Li/Nb ratio was set to 1. The molar compositions of studied materials are summarized in Table 1.

To synthesize bulk gels with composition $5Li_2O$–$5Nb_2O_5$–$90SiO_2$ (*B*-5LN) and $10Li_2O$–$10Nb_2O_5$–$80SiO_2$ (*B*-10LN), a solution of $NbCl_5$ in anhydrous ethanol, EtOH, having a molar ratio $NbCl_5$:EtOH = 1:9 was prepared in a dry box at room temperature. This solution was fluxed by dry-air for 20 min to allow the HCl removal. At the same time, a solution of $LiNO_3$ in EtOH ($LiNO_3$:EtOH = 1:9) was prepared and after the complete dissolution of $LiNO_3$, was mixed to the first one. The resulting solution was mixed with a solution of TEOS, EtOH, H_2O and HCl (TEOS:EtOH:H_2O:HCl = 1:2:4:0.01) previously stirred for 1 h at room temperature, where hydrochloric acid was added as catalyst. From this final solution transparent and homogeneous gels were obtained after a few hours. The gels were kept for two days at room temperature and then dried in air at 110 °C in an electric oven for three days, yielding transparent bulk samples for each composition. These samples were finely ground before the subsequent heat-treatments in air.

As intermediate step, to approach the films preparation, a synthesis procedure was set to obtain transparent flakes with thickness less then 0.5 mm. At this stage flakes with composition $10Li_2O$–$10Nb_2O_5$–$80SiO_2$ (*F*-10LN) and $15Li_2O$–$15Nb_2O_5$–$70SiO_2$ (*F*-15LN) were prepared. The synthesis route was the same as for

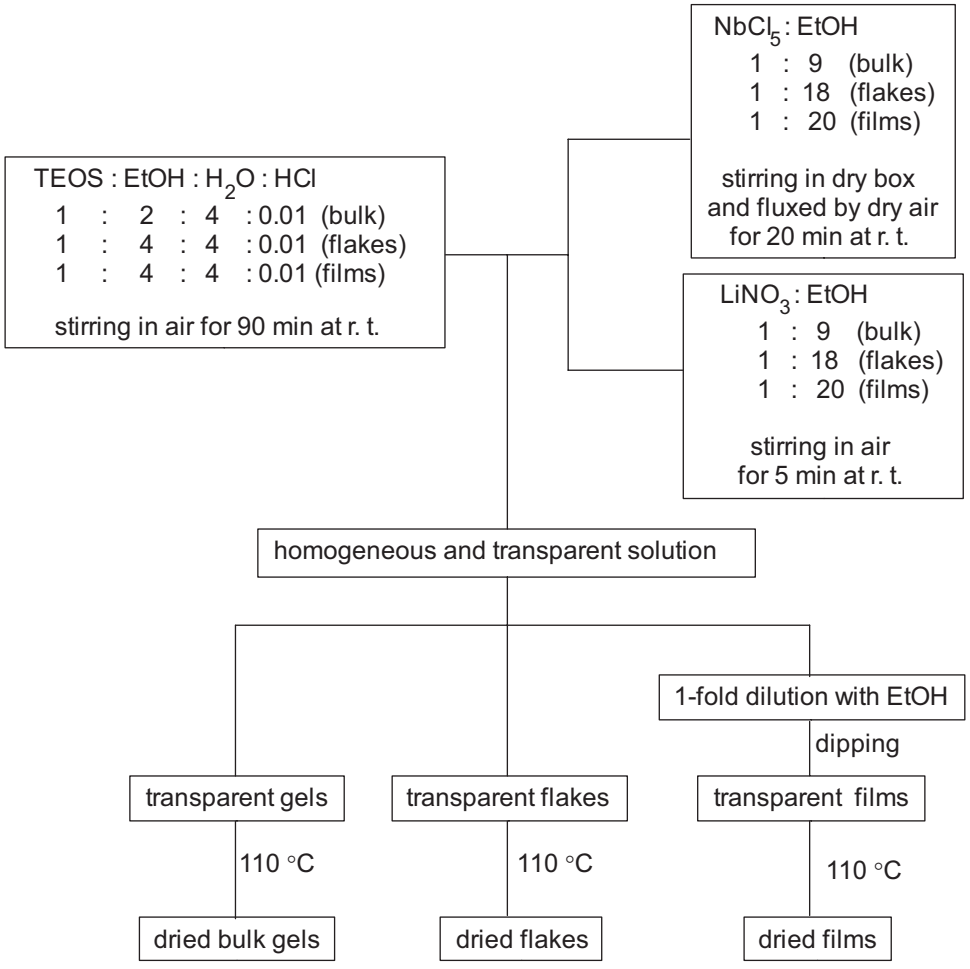

Fig. 1. Flow-chart of the synthesis procedure showing the molar ratios employed for LN-10 composition.

the bulk gel except for the EtOH amount, which was doubled in each step, to slow down the gelation process. The final solutions were stirred at room temperature for two days and then poured into a petri dish. In this condition, owing to the wide surface area, the solvents evaporation is allowed to occur and the gelation process is more similar to that taking place during the film preparation by dipping. After two days, transparent chips were obtained. They were left at room temperature for two more days and then dried at 110 °C for one day in an electric oven.

After preliminary tests, thin films with composition $10Li_2O$–$10Nb_2O_5$–$80SiO_2$ (*TF*-10LN) were prepared by dip-coating from even more diluted solutions: $NbCl_5$:EtOH = 1:20 and $LiNO_3$:EtOH = 1:20, mixed with TEOS:EtOH:H_2O:HCl = 1:4:2:0.01. The resulting clear solution was further diluted by adding EtOH to have a 50% increase of the volume. From this final solution thin films were obtained by dip-coating at room temperature on Si–SiO_2 and Al_2O_3 substrates ($10 \times 10\,mm^2$) settling the withdrawal speed of substrate at $25\,mm\,min^{-1}$ and the deposition time at 20 s. Thin films were transferred into an electric oven and heated in air, first at 110 °C for 2 h (drying step) and then at 400 °C for 3 h to allow the evacuation of solvent and residual organic molecules (stabilization step). The preparation procedure is schematically summarized in the flow-chart of Fig. 1 for the composition 10-LN.

The weight loss of the bulk samples as well as the nature and temperatures of the various reactions occurring during the heating were evaluated by a Netzsch simultaneous thermoanalyser STA 409 PC with Al_2O_3 as reference material and equipped with Al_2O_3 sample holders. The TG/DTA curves, recorded in air from room temperature up to 1000 °C at heating rate of 10 °C min^{-1}, were carried out on 50 mg of the dried gels.

The amorphous nature of the dried gels as well as the nature of the crystallizing phases formed at higher temperature were ascertained by X-ray diffraction (XRD) using a Philips diffractometer model PW1710 (Cu*K*α) at a scan rate of $1^\circ\,min^{-1}$. The films crystallization was studied by XRD using a Rigaku D-Max B diffractometer (Cu*K*α), at a scan rate of $1^\circ\,min^{-1}$ and using the Bragg-Brentano configuration. The thickness and roughness of the heat-treated films were measured by a TENCOR profilometer. The electrical properties of thin films were investigated by current–voltage measurements with a standard two probe technique. Both the applied voltage and the measured current were controlled by a Keithley 487 picoammeter. Silver electrodes were sputtered over the film surface by using planar configuration, providing active channels with length and width of 100 μm and 5 mm, respectively. Not destructivity and precision of the measurements were assured by utilizing a probe station with metallic tips mounted on micrometric slides.

3. Results and discussion

As first stage, $5Li_2O$–$5Nb_2O_5$–$90SiO_2$ (*B*-5LN) and $10Li_2O$–$10Nb_2O_5$–$80SiO_2$ (*B*-10LN) bulk gels were prepared to find the optimal conditions for the gel synthesis and the heat-treatments suitable for $LiNbO_3$ crystallization. Fig. 2 displays the TG/DTA curves recorded on bulk dried gel samples. The overall weight losses obtained by the TG curves were: 23 wt% (*B*-5LN) and 31 wt% (*B*-10LN). In each case, the majority of the weight loss takes place between room temperature and about 250 °C. In this range, on the DTA curves of both the samples, a broad endothermic peak is seen with a maximum at about 120 °C, which can be related to the evaporation from open pores of water and alcohol molecules physically trapped in the gels. No other evident transformation is seen at higher temperatures on the DTA curves and the weight loss can be considered complete at about 500 °C. On this basis,

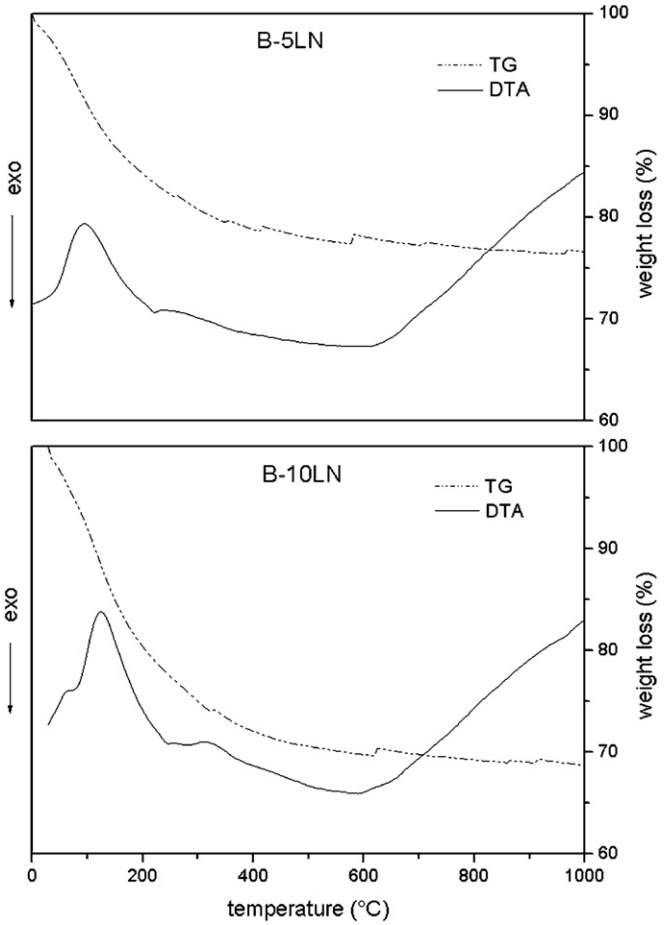

Fig. 2. TG/DTA curves of bulk gels recorded in air at $10\,K\,min^{-1}$.

from the prepared gels stable and fully amorphous xerogels were obtained by 4 hours heating at 400 °C.

To force the crystallization of the gel-derived samples, isothermal heat-treatments were performed at 650, 700, 750 and 800 °C. Each sample was slowly heated (at $5\,^\circ C\,min^{-1}$) up to the selected temperature and held 4 h. The corresponding XRD spectra are shown in Fig. 3, where the heat-treated samples are indicated by their labels followed by the temperature of the heat-treatment, e.g. *B*-5LN-650. The coherent scattering regions start to appear from the amorphous background at $2\Theta = 22.4^\circ$, on the *B*-5LN-650 spectrum. This value corresponds to the most intense peak of the T-Nb_2O_5 phase (JCPDS card 27-1312) [17]. The width of this peak suggests the growth in the amorphous matrix of crystals on nanometric scale. On the contrary, peaks related to $LiNbO_3$ (JCPDS card 85-2456) [18] start to appear in the spectrum of the *B*-10LN-650, together with that of the T-Nb_2O_5 phase. In the subsequent heating stage (750 °C) no significant differences are seen in the XRD profiles of both samples. At higher temperatures for the *B*-5LN the crystallization of a few new phases, among them $LiNbO_3$, begins, even if for this composition the T-Nb_2O_5 is the predominant phase at all the temperatures. But for the *B*-10LN sample, the intensity of $LiNbO_3$ peaks increase with the heat-treatment temperature; for this composition lithium niobate is the predominant phase at each temperature, even if small amounts of T-Nb_2O_5 and $LiNb_3O_8$ (JCPDS card 26-1176) [19] are present.

The XRD data indicate that $LiNbO_3$ amount increases with Li and Nb contents. Therefore, as this work is aimed to obtain transparent films containing $LiNbO_3$ nanocrystals as main phase, the 5LN composition was rejected since it gave a low amount of

$LiNbO_3$ and a new gel, with a composition $15Li_2O$–$15Nb_2O_5$–70-SiO_2 (15LN), has been synthesized. At this intermediate step toward the films preparation, gels were obtained as transparent flakes with composition *F*-10LN and *F*-15LN. Contrary to the bulk gel preparation, in this case the solutions, after two days stirring at room temperature, were poured into a petri dish to give a thin layer of solution. In this condition, owing to the wide surface area the solvents evaporation is allowed to occur and the gelation process is more similar to that occurring during the film preparation by dipping. The TG/DTA of the dried flakes (not reported) indicated a behavior quite similar to the bulk gels. Also in this case stable and fully amorphous samples were obtained by 4 h heating at 400 °C.

To check the $LiNbO_3$ crystallization, even the flakes samples were heated for 4 h at different temperatures (550, 600 and 650 °C). These values, lower than those of the bulk samples, have been used in order to see the very beginning of the crystallization, since in *B*-10LN sample it already starts at 650 °C. Knowing the lowest temperature value at which $LiNbO_3$ crystals grow is important to control crystals size.

The XRD spectra of the *F*-10LN and *F*-15LN samples heated 4 h at different temperatures are reported in Fig. 4. The *F*-10LN-550 is still amorphous, while the *F*-10LN-600 XRD spectrum shows an early crystallization stage with few low intensity peaks, corresponding to the most intense ones of $LiNbO_3$. In the subsequent heating stage, the crystallization of $LiNbO_3$ is enhanced even if the peaks broadness as well as the transparency of the crystallized sample point out to nanocrystallization; the average crystal size, roughly estimated by the Scherrer formula, was about 8 nm. It is worth to note that, contrary to the *B*-10LN where several crystalline phases were formed, in the *F*-10LN $LiNbO_3$ was the only crystallizing phase. As regard the *F*-15LN, the XRD spectra reported in Fig. 4 indicate that the crystallization of $LiNbO_3$ is strongly enhanced and only a small amount of $LiNb_3O_8$ is formed both at 550 and at 600 °C. The $LiNbO_3$ crystal size, increasing with the temperature, is about 24 nm at 600 °C.

The results on the flakes indicate that with 10LN composition the $LiNbO_3$ crystallization is slower but it is the only crystallizing phase, while with 15LN it is enhanced but coupled with a certain amount of $LiNb_3O_8$. Therefore, 10LN appears to be the composition

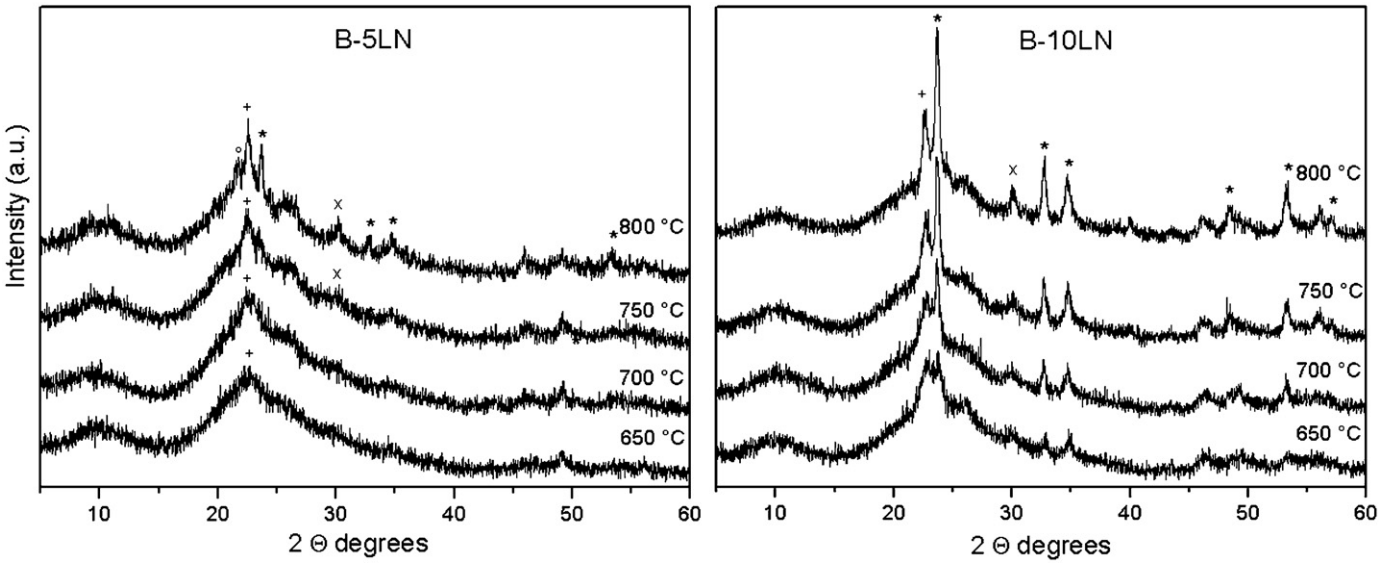

Fig. 3. XRD patterns of the bulk gels heat 4 h at different temperatures: * $LiNbO_3$, + T-Nb_2O_5, × $LiNb_3O_8$, ◦ cristobalite.

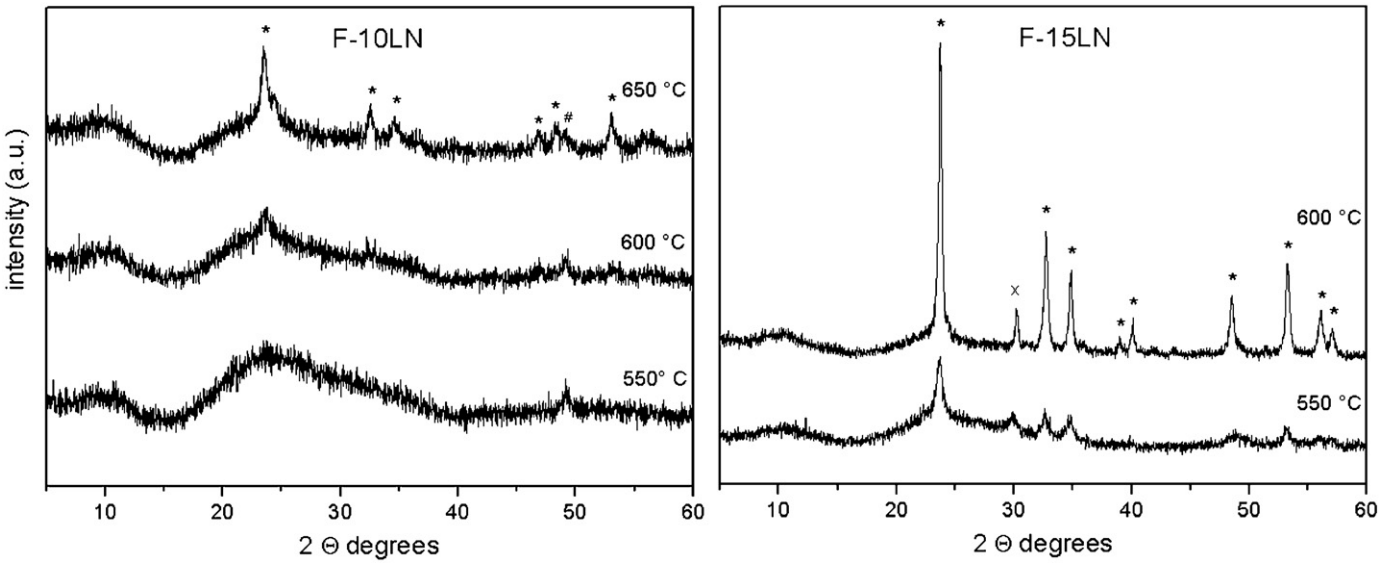

Fig. 4. XRD patterns of the flakes gels heat 4 h at different temperatures: * $LiNbO_3$, × $LiNb_3O_8$, ♯ sample holder.

more suitable to prepare thin films of $LiNbO_3$–SiO_2 nanocomposite with nanocrystals well dispersed in the silica matrix. The thin films (*TF*-10LN) were prepared by dip-coating on Si–SiO_2 substrate. The sol was diluted by EtOH to reduce its viscosity and to increase the gelation time, in order to obtain enough thin and reproducible films. The dried films, stabilized by 3 h heating at 400 °C, were fully amorphous and crack-free and the film thickness, measured by a profilometer, was about 400 nm. In the *TF*-10LN films, $LiNbO_3$ nanocrystals were obtained by heat-treatment in the range 600–800 °C. In Fig. 5 the XRD spectrum of the sample heated 2 h at 800 °C is reported, it is seen that only $LiNbO_3$ nanocrystals are formed with an average size 27 nm, as obtained by the Scherrer equation.

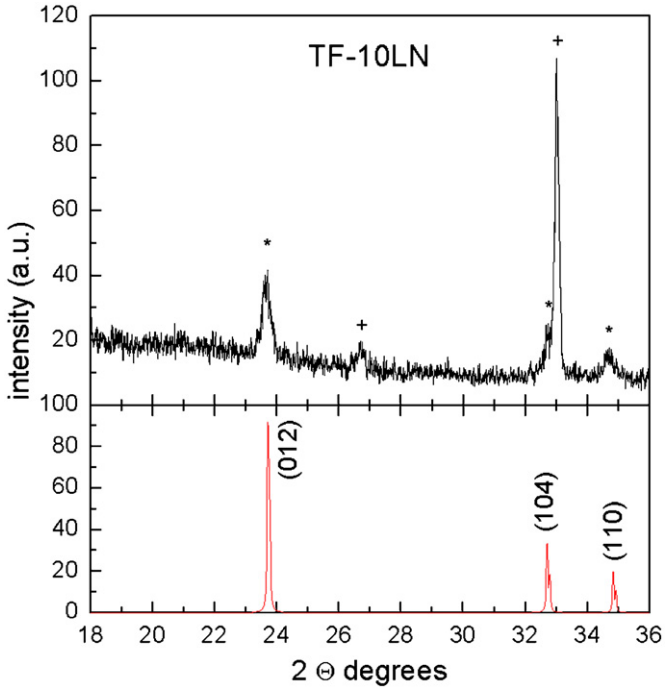

Fig. 5. XRD pattern of the thin film on Si–SiO_2 substrate heated 2 h at 800 °C. * $LiNbO_3$, + substrate. In the bottom panel the powder spectra calculated for the $LiNbO_3$ (*R3c* space group, $a = 5.148$ Å and $c = 13.863$ Å) is reported.

Films of the same composition and thickness were also prepared on Al_2O_3 (sapphire) r-plane substrate. The XRD measurements across the most intense (012) reflection of the $LiNbO_3$ rhombohedral structure is reported in Fig. 6(a) of heat-treated films at 400–700 °C. Films annealed at 400 °C have not evidenced the formation of the nanocrystals, while the presence of the (012) reflection in the case of films annealed at 600 and 700 °C confirms the fundamental role of the annealing temperature in the formation of the nanocrystals. Thought the very strong diffraction signal of the substrate prevents the careful fit of the (012) peak profile of the film, the average grains size estimated by the Scherrer equation is reported in Table 2. The data show that the selected heat-treatments favor the nanometric grains formation and that the grains size enhances with the annealing temperature, ranging from about 10–20 nm. Correspondingly, the shift of the (012) peak positions toward lower angles in the XRD spectra, evidences an increasing of the lattice spacing towards the bulk value ($d_{012} = 3.749$ Å). The extracted lattice spacings are also reported in Table 2. This effect is in agreement with the strain relaxation in the nanocrystals, which occurs when the grains dimension enhances thanks to the higher annealing temperature.

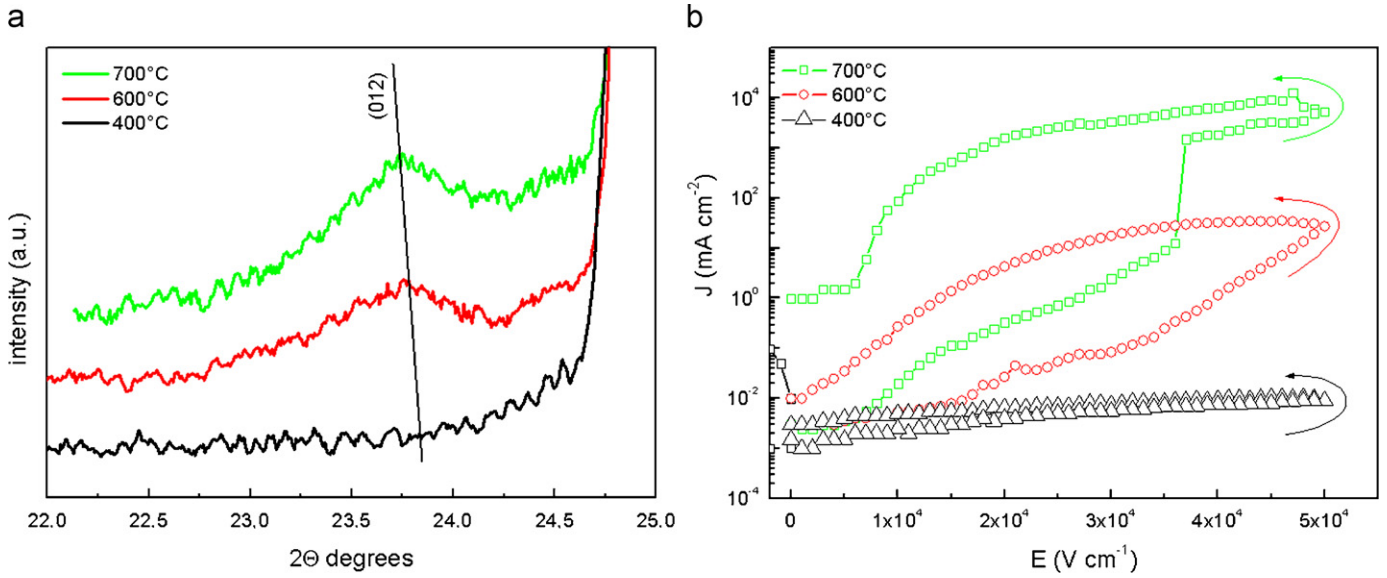

Fig. 6. (a) XRD spectra of the heat-treated films at 400, 600 and 700 °C deposited on Al_2O_3 substrate across the (012) reflection. The straight line is a guide for eyes, (b) *J*–*E* measurements of the same films during a voltage sweep from 0 to +500 V and +500 to 0 V. Arrows indicate the direction of the voltage sweep.

Table 2
Main structural and electrical parameters of the films grown on Al_2O_3 substrates annealed at different temperatures.

Sample	Annealing temperature (°C)	$LiNbO_3$ grain size (nm)	d_{012} Lattice spacing (Å)	Resistivity (Ω cm)
TF-LN10-400	400	–	–	10^9
TF-LN10-600	600	10	3.73 ± 0.01	10^6
TF-LN10-700	700	20	3.750 ± 0.005	10^4

The mean resistivity is evaluated at 400–500 V.

The electrical properties of thin films grown on Al_2O_3 substrates were also assessed by basic current–voltage (I–V) characterizations. Measurements involving different couples of electrical contacts displayed similar results, thus confirming the film spatial homogeneity concerning the electrical properties. I–V curves showed to be reproducible and stable in time, even when repeated after about six months. In Fig. 6(b), the J–E (current density versus electric field) curves of the heat-treated films at 400, 600 and 700 °C are reported. The corresponding resistivity values are summarized in Table 2. As shown, the films obtained at 400 °C without any post-annealing treatment resulted to be less conducting, with resistivity values of about $10^9\,\Omega\,cm$. On the other hand, by increasing the film annealing temperature at 600 and 700 °C, a considerable resistivity reduction (up to about five orders of magnitude) and the occurrence of highly hysteretic behaviors were observed. In particular, a direct correlation between the hysteresis in current–voltage measurements and the increase of the average grains size of $LiNbO_3$ nanocrystals has been found.

More detailed morphological and structural characterizations by atomic force microscopy and glancing XRD, have been reported in Ref. [20], where the film electrical transport properties are also further discussed.

4. Conclusions

Nanostructured thin films containing lithium niobate nanocrystals embedded in a silica matrix have been obtained in air and at room temperature by an accurate control of gel composition and synthesis parameters. The preparation conditions favor the growth of stoichiometric $LiNbO_3$ nanocrystals as only crystalline phase in the films. The crystal size remains on nanometric scale (<30 nm) even for 2 h annealing at 800 °C. The electrical transport properties of films grown on Al_2O_3 substrates and annealed at 700 °C show evidences of electrical bistability, basically related to the increased nanocrystals dimension.

References

[1] P. Lerner, C. Legras, J.P. Dumas, J. Cryst. Growth 3–4 (1968) 231.
[2] R. Fernández-Ruiz, V. Bermùdez, Chem. Mater. 16 (2004) 3593.
[3] J.K. Krebs, U. Happek, Appl. Phys. Lett. 87 (2005) 251910.
[4] S. Hirano, K. Kato, J. Non-Cryst. Solids 100 (1988) 538.
[5] S. Hirano, T. Yogo, W. Sakamoto, Y. Takeichi, S. Ono, J. Eur. Ceram. Soc. 24 (2004) 435 and references therein.
[6] Z. Cheng, K. Ozawa, A. Miyazaki, H. Kimura, J. Am. Ceram. Soc. 88 (2005) 1023.
[7] H.C. Zeng, S.K. Tung, Chem. Mater. 8 (1996) 2667.
[8] E.R. Camargo, M. Kakihana, Chem. Mater. 13 (2001) 1905.
[9] M. Liu, D. Xue, K. Li, J. Alloy Compd. 449 (2008) 28.
[10] A.V. Chadwick, M.J. Pooley, S.L.P. Savin, Phys. Status Solidi C 2 (2005) 302.
[11] A.V. Chadwick, S.L.P. Savin, L.A. O'Dell, M.E. Smith, J. Phys. Condens. Matter 18 (2006) L163.
[12] E. Bescher, Y. Xu, J.D. Mackenzie, J. Appl. Phys. 89 (2001) 6341.
[13] M.P.F. Graça, M.G. Ferreira da Silva, M.A. Valente, J. Non-Cryst. Solids 351 (2005) 2951.
[14] M.P.F. Graça, M.G. Ferreira da Silva, A.S.B. Sombra, M.A. Valente, J. Non-Cryst. Solids 352 (2006) 1501.
[15] M.P.F. Graça, M.G. Ferreira da Silva, M.A. Valente, J. Sol–Gel Sci. Technol. 42 (2007) 1.
[16] A. Aronne, E. Marenna, V. Califano, E. Fanelli, P. Pernice, M. Trifuoggi, A. Vergara, J. Sol–Gel Sci. Technol. 43 (2007) 193.
[17] JCPDS card 27-1312, International Centre for Diffraction Data.
[18] JCPDS card 85-2456, International Centre for Diffraction Data.
[19] JCPDS card 26-1176, International Centre for Diffraction Data.
[20] E. Marenna, C. Aruta, E. Bontempi, A. Cassinese, P. Colombi, L.E. Depero, P. Pernice, A. Aronne, J. Sol–Gel Sci. Technol. 49 (2009) 106.